Cutting to Measure the Elasticity and Fracture of Soft Gels

Journal:	*Soft Matter*
Manuscript ID	SM-ART-06-2020-001174.R1
Article Type:	Paper
Date Submitted by the Author:	19-Aug-2020
Complete List of Authors:	Duncan, Teresa ; National Institute of Standards and Technology, Materials Science and Engineering Division Sarapas, Joel; National Institute of Standards and Technology, Materials Science and Engineering Division Defante, Adrian; National Institute of Standards and Technology, Materials Science and Engineering Division Beers, Kathryn; National Institute of Standards and Technology, Materials Science and Engineering Division Chan, Edwin; National Institute of Standards and Technology, Materials Science and Engineering Division

SCHOLARONE™
Manuscripts

Journal Name

ARTICLE TYPE

Cutting to Measure the Elasticity and Fracture of Soft Gels[†]

Teresa T. Duncan,[a] Joel M. Sarapas,[a] Adrian P. Defante,[a] Kathryn L. Beers[a] and Edwin P. Chan[a*]

The fracture properties of very soft and/or brittle materials are challenging to measure directly due to the limitations of existing fracture testing methods. To address this issue, we introduce a razorblade-initiated fracture test (RIFT) to measure the mechanical properties related to fracture for soft polymeric gels. We use RIFT to quantify the elasticity, crack initiation energy, and the fracture energy of gellan hydrogels as a function of gellan concentration. Additionally, we use RIFT to study the role of friction in quantifying the fracture properties for poly(styrene-*b*-ethylene butadiene-*b*-styrene) gels as a function of test velocity. This new method provides a simple and efficient means to quantify the fracture properties of soft materials.

1 Introduction

For a crack to propagate, the applied energy required for crack growth (G) must exceed its fracture energy (G_c), i.e., $G \geq G_c$.[1] Methods used to measure G can be divided into two categories: 1) ones that use a pre-notch as an initial crack and 2) ones that do not require a pre-notch. Methods requiring an initial crack include the pure shear test,[2] the simple extension test,[2] the single edge crack test,[3] and the tearing test.[4] Tearing and cutting energies can be simultaneously measured by employing a razorblade in a y-shaped cutting experiment, as performed on rubbers[5] and softer elastomers.[6]

Less common are methods that directly measure fracture energy by initiating and propagating a crack without a pre-notch. The advantage is the convenience of these methods as they typically require minimal sample preparation. For instance, a puncture-based test using a spherically-tipped indenter was recently developed that measures the critical force required to initiate and propagate a crack for soft gels.[7,8] Although not considered a traditional fracture test, cavitation rheology has been used to measure the fracture energy of soft gels in cases when the critical pressure required for fracture is less than that required for nonlinear elastic expansion of the material.[9–12] The food industry has a long history of using wire cutting to measure the fracture behavior of foods such as cheese, and this method has been extended to soft solids.[13,14] The advantage of wire cutting is that the surface area of the wire creates a well-defined and constant
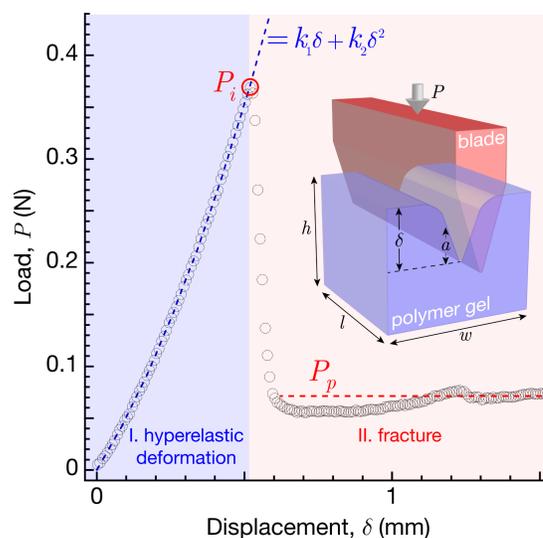
Fig. 1 The razorblade-initiated fracture test (RIFT) experiment. Representative load P vs. δ results of the test for a gellan gel. The inset is a schematic of the RIFT test illustrating the geometry of the sample, the deformation of the sample (δ) and the crack (a).

contact area with the material thus reducing the effects of friction to the fracture process, which can be significant in some soft materials. A major drawback of the wire-cutting method is that the mechanical compliance of the wire can be quite high such that extreme pretensioning of the wire is required to effectively cut the material.

In this work, we present an alternative measurement technique called razorblade-initiated fracture test (RIFT), which is an indentation-based approach that uses a razorblade to deform and

then cut a sample in order to measure the elasticity, crack initiation energy and fracture energy in one single test (Fig. 1). The advantages of RIFT is that it requires: 1) minimal sample preparation, and 2) no clamping of the sample thus making it an ideal technique for cutting extremely soft or brittle materials that would be damaged upon clamping. We primarily use gellan hydrogels as a model material to highlight the measurement capabilities of RIFT. Gellan gels have similar properties to agar hydrogels, but form gels at lower concentrations of polysaccharide, and have therefore been used in a range of applications as a cost-effective substitute to agar. We demonstrate that RIFT can be used to characterize the elasticity and fracture properties of gellan gels with a range of mechanical properties that is controlled by varying the concentration of gellan relative to the water content. We also studied the fracture behavior of poly(styrene-b-ethylene butadiene-b-styrene) (SEBS) gels, which is another physically-associating gel, to show the contributions of friction to the fracture behavior as measured by RIFT.

2   Experimental

Gellan gels were prepared by combining gellan and water in 20 mL scintillation vials. The mixture was mixed with a spatula, sealed and then heated to 90 °C with stirring. After 10 min, a spatula was used to disperse any remaining inhomogeneities, and the mixture was heated for an additional 10 min without stirring. Once the solution appeared homogeneous and bubble-free, it was poured into a 7.4 cm × 2.2 cm × 0.5 cm Teflon mold and covered with a glass slide to allow it to solidify. Gellan concentrations ranging from 2 % by mass fraction to 5 % by mass fraction were prepared corresponding to sample names G_2 to G_5. Mechanical tests were performed on each sample after 24 h of preparing the gel.

We also studied the fracture behavior of SEBS gels using RIFT to explore the effects of friction. SEBS gels were prepared by combining 10 % by mass of SEBS block copolymer (Vector® 4411A, Dexco Polymers) with 90 % by mass of mineral oil (MAL6358 paraffin oil, Macron Chemicals). The solution was prepared by heating the mineral oil to 115 °C on a hot plate in a glass beaker with a Teflon stir bar. Solid pellets of SEBS were added in slowly, allowing the polymer to dissolve into the mixture. The Teflon mold, with dimensions of 7.4 cm × 2.2 cm × 0.5 cm, was placed in an oven at 80 °C to prevent initial gelation upon contact and formation of air bubbles. The solution was poured to fill each mold as quickly as possible to avoid premature gelation. The solution was then left in the oven for 10 min, removed, and allowed to gel at room temperature. The solidified samples were removed from the mold and cut into the appropriate lengths for testing.

The Young's modulus (E) of the gels was also measured using contact adhesion testing (CAT).[15] A spherical glass probe, of radius $R = 1$ mm, was brought into contact with the sample at a crosshead speed of 5 μm/s up to a compressive load $\approx$ 2 mN. A Leica DMIRE2 inverted microscope, coupled to a JAI BM-500GE camera, was used to image the contact area (πr^2) at the applied displacement (δ) and corresponding load (P) values. A geometric confinement correction factor for P was used to account for the influence of substrate stiffness that is quanti-

fied by the ratio of the contact radius and sample thickness (h). For $r/h < 0.5$, $P' = P(1 - r/h)$.[16] By assuming the material to be isotropic and incompressible, E was determined from the slope ($= E^* = E/(1 - \nu^2)$) of an effective stress (P'/r^2) versus effective strain ($(2\delta/r) + (2r/3R)$) curve. We note that E measured by CAT is termed E_{CAT} and the ones measured by RIFT is simply E.

For the RIFT experiments, a texture analyzer (Stable Micro Systems TA-XT2i HR, Texture Technologies Corp.) with a 5 kg load cell was used to measure P and δ as a razorblade (VWR, surgical carbon steel, single edged No. 9) was driven into the gels with defined cut lengths (l). The radius of curvature (R) of the razorblades was measured using an optical profilometer (Zygo NewView 7300, Zygo Corporation) with $R = 8.6$ μm ± 0.5 μm (See Supporting Info, Fig. S1a). Each gel was removed from the Teflon mold and then cut into specimens with dimensions of $l = 10$ mm, 15 mm, 20 mm and 25 mm, with constant width ($w = 2.2$ cm) and thickness ($h = 0.5$ cm). The exact l for each sample was measured with a caliper before cutting. Fresh blades were used for each sample since blade dulling is known to affect fracture measurements.[17,18] RIFT measurements were first collected at various crosshead speeds ($v = 0.1$ mm/s, 0.5 mm/s and 1.0 mm/s), with the δ vs. time curve measured directly from the instrument, in order to optimize the deformation rate used for further experiments. We found that a $v = 0.1$ mm/s was too slow, leading to periodic fluctuations in the measured force potentially due to stick-slip events between the blade and hydrogel, whereas speeds of 0.5 mm/s and 1.0 mm/s produced consistent results (See Supporting Info, Fig. S1 and S2). A speed of 0.5 mm/s was used for all RIFT measurements on gellan gels presented herein. Crosshead speeds of 0.01 mm/s, 0.1 mm/s and 1 mm/s were used for the SEBS gels. The crack initiation energy (Γ) was extrapolated from the slope of the maximum P before crack initiation (P_i) vs. l curve. The fracture energy (G_c) was extrapolated from the slope of the average P during crack propagation (P_p) vs l curve.

3   Results and Discussion

Fig. 1 is a representative P vs. δ plot of a gellan gel measured using RIFT. In this first part of the test (highlighted in blue), the blade is elastically indenting the sample. The deformation behavior is nonlinear elastic, and is consistently observed across all of the materials investigated. This mechanical response is similar to other indentation tests involving deformation of compliant materials, including the indentation of elastomers by a wedge[19] and puncture of gels with a needle.[8,20] For such tests, the relationship between P and δ was empirically defined as,

$$P = k_1\delta + k_2\delta^2 \tag{1}$$

where k_1 and k_2 are fitting constants related to the stiffness of the material. For indentation tests involving a slender rod indenting a soft gel, it has been shown that k_1 is proportional to E of the gel.[8] Here, we calculate the elasticity of the gels using RIFT by assuming that,

$$E = \frac{k_1/l}{c_1} \tag{2}$$
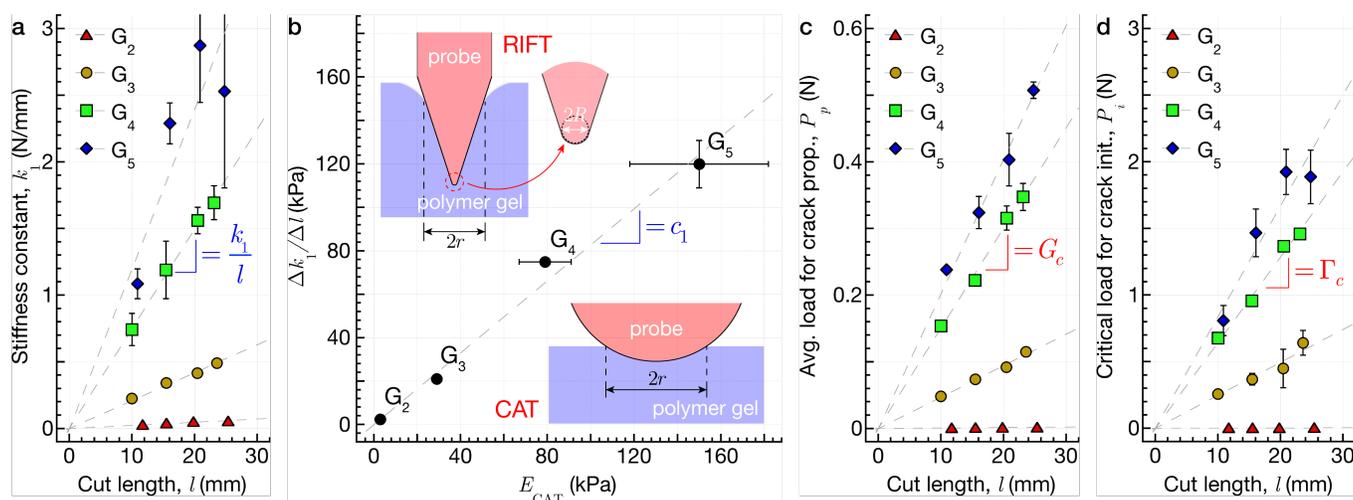
Fig. 2 Summary of the RIFT results for the gellan gels. a) Stiffness constant (k_1) vs. cut length (l) as a function of gellan content. We use the slope of this plot ($= k_1/l$) to determine the elasticity of the gellan gels. b) Comparison of k_1/l measured by RIFT vs. elastic modulus (E_{CAT}) measured by contact adhesion test (CAT). c) Avg. load for crack propagation (P_p) vs. l as a function of gellan content. The slope of each curve corresponds to the fracture energy (G_c). d) Critical load for crack initiation (P_i) vs. l as a function of gellan content. The slope of each curve corresponds to the crack initiation energy (Γ_c). Error bars correspond to one standard deviation.

For each sample, the stiffness parameter k_1 was experimentally determined from the P vs. δ plot of the RIFT test by fitting the first part of the curve with Eq. (1) (Fig. 1). Next, we determine the parameter k_1/l from the slope of k_1 vs l plot as shown in Fig. 2a. We define c_1 as a geometric correction factor that is related to the specific blade geometry thus different blades will have different values for c_1. Specifically, we determine c_1 by comparing k_1/l to the elasticity values (E_{CAT}) measured from CAT (Fig. 2b) and find that they are proportional to each other with a proportional constant $c_1 \approx 0.83$. Finally, E values for the gellan gels are calculated by substituting k_1/l and c_1 into Eq. (2).

In the second part of the RIFT test (highlighted in red), the blade continues to deform the gel but now punctures the material thus leading to the development of a critical force for crack initiation (P_i) (Fig. 1). Past this critical point, the crack propagates into the gel at a constant value of P_p until the gel completely fractures into two halves. From Williams and Patel,[21] the energy balance for this cutting process is defined as,

$$dU_{ext} = dU_f + dU_\mu + dU_p \qquad (3)$$

The external work is $dU_{ext} = P_p d\delta$. The fracture energy due to cutting is $dU_f = lG_c d\delta$, the energy dissipated due to friction is $dU_\mu = Sd\delta$ (with S being the shear force), and the energy due to plastic deformation is dU_p. Eq. (3) is a result of these three contributions but we can simplify the expression by making certain assumptions of the cutting process. The simplest scenario is when friction between the blade and sample, as well as plastic deformation, can be ignored. Here, $dU_p = dU_\mu = 0$ and Eq. (3) simplifies to,

$$P_p d\delta = lG_c d\delta$$
$$\implies \frac{P_p}{l} = G_c \qquad (4)$$

In this case, Eq. (4) suggests that G_c can be extrapolated by measuring P_p as a function of l. The RIFT results (see Supporting Info, Fig. S1 and S2) for our gellan gels all display this behavior where P_p remains constant with increasing δ after puncture. These results suggest that friction and plastic deformation are negligible since friction should increase with the contact area between the blade and the sample, while plastic deformation should increase with deformation volume.

Table 1 Materials properties as a function of gellan concentration (c) of gellan gels extracted from RIFT. The materials properties include elastic modulus (E), fracture energy (G_c), crack initiation energy (Γ_c) and elasto-fracture length (G_c/E). Error values correspond to one standard deviation.

	c (mass %)	E (kPa)	G_c (J/m^2)	Γ_c (J/m^2)	G_c/E (μm)
G_2	2	2.85 ± 0.12	0.07 ± 0.00	0.14 ± 0.01	≈ 25
G_3	3	25.3 ± 0.51	4.73 ± 0.01	24.8 ± 1.32	≈ 187
G_4	4	90.3 ± 1.09	15.0 ± 0.19	64.3 ± 1.16	≈ 166
G_5	5	144 ± 13.2	20.2 ± 0.41	83.5 ± 4.64	≈ 140

We use Eq. (4) to determine G_c for the gellan gels. Specifically, we plot P_p vs. l as a function of gellan concentration (c) and extrapolate G_c from the slope of this plot (Fig. 2c). Additionally, we estimate Γ_c by assuming that $\Gamma_c \approx P_i/l$ (Fig. 2d). The values for E, G_c and Γ_c for the gellan gels are summarized in Table 1. Also included in this table is the elasto-fracture length ($= G_c/E$), which is an estimate of the critical flaw size of the gel.[22] Based on the measured radius of curvature of the razorblades, $R < G_c/E$, which indicates that the fracture behavior of these gels should be insensitive to the defects in the gels.

The results show that E, G_c and Γ_c (Table 1) all increase with increasing c. The E values for the gellan gels (Fig. 3a) are similar to previously reported results.[23] It is interesting to note that the relationship between E and c do not follow the traditional scaling for a polymer gel ($E \sim c^\alpha$) that consists of random coils linked at

crosslinks with $\alpha \approx 2.3$.[24] Instead, we find that $\alpha \approx 4.4$, which is similar to the results reported by Kawai *et al.*[25] for gellan gels and by Watase *et al.*[26] for agarose gels. Although gellan forms random coils at elevated temperatures ($\approx 80\,^\circ$C) when dissolved in water, the polymer converts into a double-helical structure upon cooling. These helical structures are thought to aggregate into bundles that are separated by segments of sterically-hindered polysaccharide coils. The short polysaccharide coils are stiffer than those described by rubber theory, and may be responsible for an increase in α.[26] Another possible reason is the presence of trace ions in the naturally-occurring polysaccharide. Monovalent (Na$^+$ and K$^+$) and divalent (Ca^{2+}) ions decrease repulsion by screening anionic charges on the polymer backbone, thereby increasing aggregation. Divalent cations are especially effective in increasing the strength of gellan gels.[27]
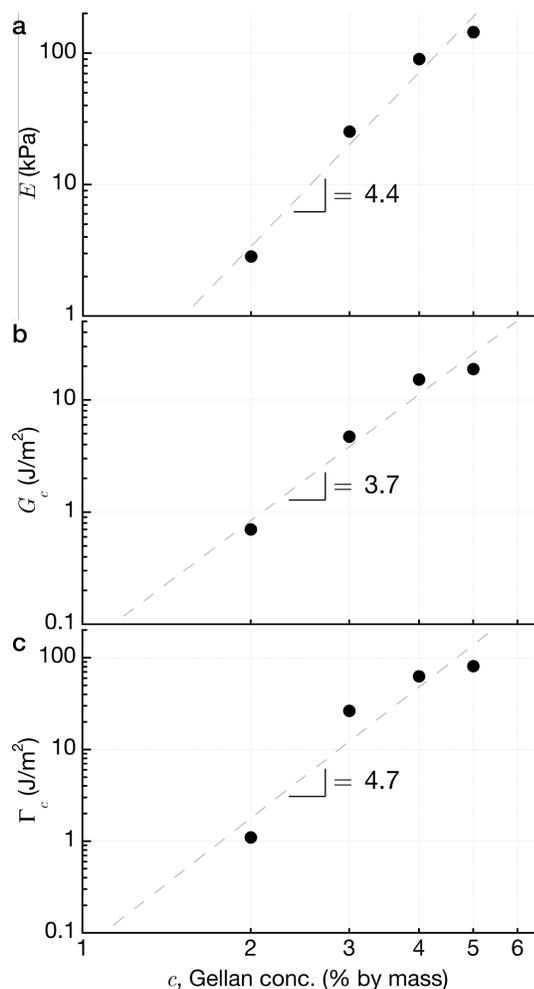
Fig. 3 a) Elastic modulus (E) as a function of gellan concentration (c). b) Fracture energy (G_c) as a function of c. c) Crack initiation energy (Γ_c) as a function of c.

Figure 3b summarizes the effect of gellan concentration on the fracture behavior of gellan gels. These values are comparable to the fracture energies for other gels with similar polymer mass fraction.[10,20,28] We see that the fracture energy increases by over an order of magnitude when we increase c from 2 % by mass to 5 % by mass. This is a significant increase in fracture energy as

a function of polymer concentration, and cannot be explained by the classic Lake-Thomas theory for fracture since the theory predicts that $G_c \sim c^\beta$ with $\beta = 0.21$ to 0.25.[10,28] An alternative fracture mechanism based on viscoplasticity was proposed by Baumberger and coworkers for gelatin gels.[29] Here, the fracture process involves chain pullout from the crosslinks followed by diffusion of the chains through the polymer mesh until they completely disengage from the polymer network. As demonstrated previously by Frieberg and coworkers,[10] the chain disengagement process can be described as $G_c \sim E/D_c$ where D_c is the cooperative diffusion coefficient of the polymer chain in solution. We note that the migration of polymer chains through the polymer mesh contributes to the mechanism of crack propagation here because of the quasi-static nature of the mechanical test coupled with the low polymer concentration. We expect that this mechanism becomes insignificant at higher deformation rates or when the polymer concentration is sufficiently high such that the Lake-Thomas theory of fracture becomes the dominant mechanism.[10] We can estimate the concentration-dependent scaling relationship for D_c from the results in Fig. 3 to find that $E \sim c^{4.4}$ and $G_c \sim c^{3.7}$. Combining these three expressions, we find that $D_c \sim E/G_c \sim c^{0.7}$, which is similar to the predictions by De Gennes ($D_c \sim c^{0.75}$) for the cooperative diffusion of a polymer chain through a gel network.[30] The crack initiation energy also increases with gellan concentration (Fig. 3c) and scales as $\Gamma_c \sim c^{4.7}$. This scaling is different from the scaling for G_c, which suggests that the mechanisms of crack initiation is different from the ones that govern crack propagation for soft materials.[8] As there are limited studies that measures both G_c and Γ_c for soft materials, we cannot comment on the scaling exponent for Γ_c. However, the values for Γ_c is about an order of magnitude larger than G_c, which is consistent to recent work on the puncture behavior of other soft gels.[7,8]

To illustrate the effects of friction, we use RIFT to measure the fracture behavior of SEBS gels as a function of crosshead speed ($v = \mathrm{d}\delta/\mathrm{d}t$) of the blade. Representative P vs. δ results for the SEBS gels as a function of v is shown in Fig. 4. In the first part of the test prior to puncture, the blade elastically deforms the SEBS gel in a manner that is similar to the gellan gels. We again characterize this indentation behavior with Eq. (1) to determine the elasticity of the material. Across all the crosshead speeds studied, we find that $k_1/l \cong 9.3$ kPa (Fig. 5a) thus indicating that $E \approx 11.8$ kPa for the SEBS gels, which is very similar to results obtained previously.[31]

In the second part of the test after puncture, the crack propagates into the sample but P_p increases with δ. We find two interesting results from these experiments. First, P_i increases with increasing v until it becomes challenging to clearly identify this critical point at the highest speed ($v = 1$ mm/s). We have conducted similar experiments on poly(dimethylsiloxane) elastomers and observed similar behavior (see Supporting Info, Fig. S3). We quantified P_i for all the crosshead speeds and the results are summarized in Fig. 5b.

Second, the magnitude of P_p increases with increasing v. We attribute this increased resistance experienced by the blade as friction thus $\mathrm{d}U_\mu = S\mathrm{d}a \neq 0$ from Eq. (3). As the blade penetrates deeper into the SEBS gel, P_p increases because the interfacial area
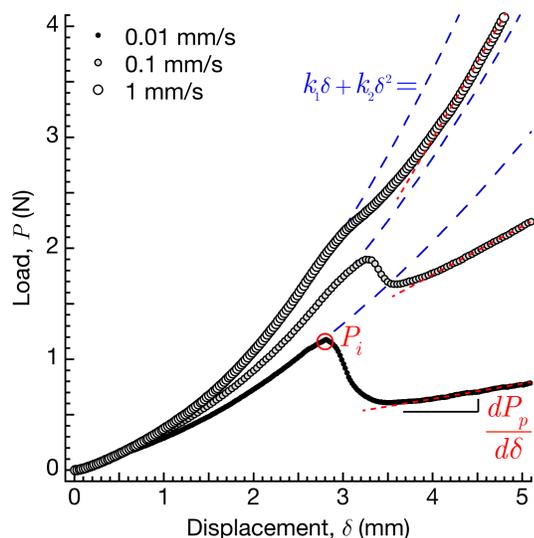
Fig. 4 RIFT results for Poly(styrene-*b*-ethylene-butadiene-*b*-styrene) (SEBS) gel. Load (P) vs. (δ) results of the SEBS gel as a function of crosshead speed of the blade.

between the blade and material increases in a proportional manner. According to Williams and Patel,[21] Eq. (3) becomes,

$$P_p d\delta = lG_c d\delta + P_s d\delta \qquad (5)$$

where P_s is the shear force acting on the blade. Williams and Patel break down P_s into the components of normal force and cutting force as a function of blade angle θ in relation to the surface of the material that the blade is in contact with.[21] Alternatively, we can estimate the shear force by assuming that it is purely based on hydrodynamic lubrication thus $P_s \approx A\eta v/h$,[32–34] where $A = 2al$ is the interfacial area between the blade and the gel, η is the dynamic viscosity, and v is crosshead speed of the blade. h is a thickness parameter that is related to the properties of the fluid layer formed between the gel and the blade. Specifically, it is velocity dependent ($h \sim v^m$) and m can range from 0.5 to 1.[34,35] We note that A is not a constant for our RIFT experiments on the SEBS gels past δ_i (at P_i) since the crack or interfacial area also increases with δ, i.e., $a = f(\delta)$. Assuming that $a \approx b\delta$ with b being a constant, $P_s \approx 2bl\delta\eta v/h$. Substituting these expressions into Eq. 5 and then taking the derivative of this expression with respect to δ yields,

$$\frac{1}{l}\frac{dP_p}{d\delta} \approx 2b\eta v^n \qquad (6)$$

with n ranging from 0 to 0.5. From the plot of $dP_p/ld\delta$ vs. v (Fig. 5c), we find that $n \cong 0.55$ which is in good agreement with the prediction for n. In regards to the RIFT experiments, these results suggest that friction plays a significant role in the crack propagation process for the SEBS gels thus limiting the extrapolation of G_c. A possible solution to mitigate the effects of friction is via lubrication of the blade. We experimented with coating the razorblade with several varieties of mineral oil but did not find this approach effective in reducing the friction between the blade and the SEBS gels.
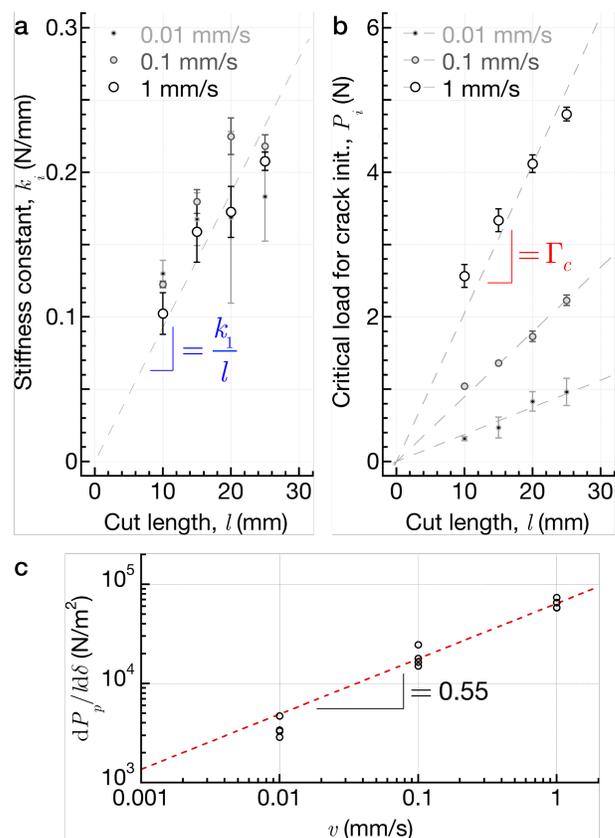
Fig. 5 Summary of the RIFT results for the SEBS gels. a) k_1 vs. l as a function of crosshead speed (v). The slope of the curves define the elasticity of the SEBS gels. b) P_i vs. l as a function of v. The slope of each curve defines Γ_c. c) $dP_p/ld\delta$ vs. v for the SEBS gels. Error bars correspond to one standard deviation.

Table 2 Summary of E and Γ_c as a function of crosshead speed (v) of SEBS gels extracted from RIFT. Error values correspond to one standard deviation.

v (mm/s)	E (kPa)	Γ_c (J/m^2)
0.01	↑	37.7 ± 2.17
0.10	11.8 ± 0.62	89.8 ± 2.52
1.00	↓	206 ± 10.4

4 Conclusions

In this work, we presented the RIFT fracture test as a simple measurement approach for characterizing the fracture properties of soft gels. In a single test, RIFT was able to measure the elasticity (E) and fracture properties (G_c and Γ_c) of gellan hydrogels as a function of gellan concentration. Both E and G_c were found to increase with increasing gellan concentration but their scaling relationships with concentration were found to be different, which cannot be explained based on the classic Lake-Thomas theory for fracture. Instead, the scaling relationships suggest that a viscoelastic fracture process is a possible mechanism of fracture for these materials. These results highlight the importance of measuring the fracture properties of soft materials directly, rather than relying on E to infer on its toughness.

Friction can play a significant role in the fracture behavior of

gels as evidenced by the RIFT results for the SEBS gels. While the RIFT test can measure E and Γ_c of the SEBS gels as a function of testing velocity, it was unable to quantify G_c. In general, RIFT can only reliably measure E for crosslinked polymers and elastomers due to the significant role of friction between the blade and the material. Future development of RIFT will be focused on making it a high-throughput measurement for screening mechanical properties of soft materials. Specifically, we will study the effects of razorblade geometry and materials composition in a combinatorial manner. Systematic variation of the razorblade geometry will enable us to control the interfacial area of the blade to control the effects of friction. Coupling geometric changes of the razorblade (i.e., radius of curvature) with compositional variation of the material will enable us to investigate the size-scale effects on the fracture process to identify the "flaw-sensitive" and "flaw-insensitive" fracture regimes for soft materials.

Conflicts of interest

Certain instruments and materials are identified in this paper to adequately specify the experimental details. Such identification does not imply recommendation by the National Institute of Standards and Technology (NIST); nor does it imply that the materials are necessarily the best available for the purpose.

Acknowledgements

Notes and references

1 R. Long and C.-Y. Hui, *Soft Matter*, 2016, **12**, 8069–8086.

2 R. S. Rivlin and A. G. Thomas, *J. Polym. Sci.*, 1953, **10**, 291–318.

3 H. W. Greensmith, *J. Appl. Polym. Sci.*, 1963, **7**, 993–1002.

4 A. N. Gent, *Langmuir*, 1996, **12**, 4492–4496.

5 G. J. Lake and O. H. Yeoh, *Int. J. Fract.*, 1978, **14**, 509–526.

6 B. Zhang, C.-S. Shiang, S. Yang and S. Hutchens, *Exp. Mech.*, 2019, **59**, 517–529.

7 S. Fakhouri, S. B. Hutchens and A. J. Crosby, *Soft Matter*, 2015, **11**, 4723–4730.

8 S. Rattan and A. J. Crosby, *ACS Macro Lett.*, 2019, **8**, 492–498.

9 S. B. Hutchens, S. Fakhouri and A. J. Crosby, *Soft Matter*, 2016, **12**, 2557–2566.

10 B. R. Frieberg, R.-S. Garatsa, R. L. Jones, J. O. Bachert, B. Crawshaw, X. M. Liu and E. P. Chan, *Soft Matter*, 2018, **14**, 4696–4701.

11 M. P. Milner and S. B. Hutchens, *Extreme Mech. Lett.*, 2019, **28**, 69–75.

12 S. Yang, D. Bahk, J. Kim, A. Kataruka, A. C. Dunn and S. B. Hutchens, *Int. J. Fract.*, 2019, **219**, 89–99.

13 S. M. Goh, M. N. Charalambides and J. G. Williams, *Eng. Fract. Mech.*, 2005, **72**, 931–946.

14 E. Reyssat, T. Tallinen, M. Le Merrer and L. Mahadevan, *Phys. Rev. Lett.*, 2012, **109**, 244301.

15 N. K. Nadermann, E. M. Davis, K. A. Page, C. M. Stafford and E. P. Chan, *Adv. Mater.*, 2015, **27**, 4924–4930.

16 A. J. Crosby, K. R. Shull, H. Lakrout and C. Creton, *J. Appl. Phys.*, 2000, **88**, 2956–2966.

17 C. T. McCarthy, M. Hussey and M. D. Gilchrist, *Eng. Fract. Mech.*, 2007, **74**, 2205–2224.

18 C. T. McCarthy, A. N. Annaidh and M. D. Gilchrist, *Eng. Fract. Mech.*, 2010, **77**, 437–451.

19 B. Setiyana, R. Ismail, J. Jamari and D. J. Schipper, AIP Conference Proceedings, 2016, p. 020078.

20 S. Rattan and A. J. Crosby, *Extreme Mech. Lett.*, 2018, **24**, 14–20.

21 J. G. Williams and Y. Patel, *Interface Focus*, 2016, **6**, 20150108.

22 C. Creton and M. Ciccotti, *Rep. Prog. Phys.*, 2016, **79**, 046601.

23 G. Ferruzzi, N. Pan and W. Casey, *Soil Science*, 2000, **165**, 778–792.

24 M. Rubinstein and R. H. Colby, *Polymer Physics*, Oxford University Press, USA, 1st edn, 2003.

25 S. Kawai, Y. Nitta and K. Nishinari, *J. Appl. Phys.*, 2007, **102**, 043507.

26 M. Watase, K. Nishinari, A. H. Clark and S. B. Ross-Murphy, *Macromolecules*, 1989, **22**, 1196–1201.

27 E. R. Morris, K. Nishinari and M. Rinaudo, *Food Hydrocoll.*, 2012, **28**, 373–411.

28 S. Kundu and A. J. Crosby, *Soft Matter*, 2009, **5**, 3963.

29 T. Baumberger, C. Caroli and D. Martina, *Eur. Phys. J. E.*, 2006, **21**, 81–89.

30 P. G. De Gennes, *Macromolecules*, 1976, **9**, 594–598.

31 S. Mishra, R. M. B. Prado, S. Zhang, T. E. Lacy, X. Gu and S. Kundu, *J. Polym. Sci. B Polym. Phys.*, 2019, **57**, 1014–1026.

32 B. N. J. Persson, *Surf. Sci. Rep.*, 1999, **33**, 83–119.

33 T. Kurokawa, T. Tominaga, Y. Katsuyama, R. Kuwabara, H. Furukawa, Y. Osada and J. P. Gong, *Langmuir*, 2005, **21**, 8643–8648.

34 Y. A. Meier, K. Zhang, N. D. Spencer and R. Simic, *Langmuir*, 2019, **35**, 15805–15812.

35 G. Kagata, J. P. Gong and Y. Osada, *J. Phys. Chem. B*, 2002, **106**, 4596–4601.